Repair-Based Design of Composite Structures: Scarf Repair

Samaneh Tashi [a], Ali Abedian [a, *]

[a] Aerospace Engineering Department, Sharif University of Technology, Azadi Street, Tehran Iran PO Box: 11365-11155

[*] Corresponding Author: Ali Abedian, Associate Professor, Email: abedian@sharif.edu, Phone Number: +98- 21-66168166, Mobile Number:

First Author: Samaneh Tashi, PhD Student, Email: Samaneh_tashi@ae.sharif.edu, Phone Number: +98- 21-66166322, Mobile Number:

Abstract

Satisfying Design Limit Load for scarfed laminate and Design Ultimate Load for repaired laminate are required for certifying adhesively bonded repair. These regulations in association with contradictory influence of scarf angle on DLL and DUL makes the certification of a scarf repair a sophisticated procedure. Current study is dedicated to obtain ultimate strength of quasi-isotropic pristine laminates and their scarf joints with the aim of investigating the effect of scarf repair performance of a laminate on its design considerations using FEM. The results showed scarf joint strength is substantially affected by the way plies shuffle in quasi-isotropic laminates. Following the conventional design guideline to stack plies of composite laminate cannot favorably affect the strength of scarf joint of that laminate. Considering the scarf repair efficiency as one of the principles to design a laminate provides the opportunity for satisfying DUL and DLL, enhance the probability of approval of a scarf repair.

Keywords: Scarf Joint, FEM, Design Philosophy, Airworthiness Regulations, Composite Structure

1. Introduction

The demand for lower fuel consumption has made composite materials popular in the aerospace industry to the extent that the primary structures of new-generation aircrafts have mostly been composed of composites. Although primary and secondary composite components are rapidly replacing their metallic counterparts in the aviation industry, commercial aircraft authorities have identified several safety issues that are mainly categorized as limited knowledge on composite parts behavior, technical concerns related to the unique properties of composite materials, limited standardization of composite materials, repair techniques, and lack of training and awareness of composite materials. As the structural design rules of composite parts including manufacturing processes and joining technologies are not as mature as metals, satisfying the safety and performance of composite airframes substantially demands for advanced repair techniques [1]. The scarf repair is a viable method for restoring the strength and stiffness of thick damaged parts, does not affect the aerodynamic or stealth characteristics of the airplane. However, a scarf joint, which is a 2-D projection of full 3-D scarf repair, is widely used as a representative for scarf repair in most of the available experimental and numerical research works.

Jones and Graves [2] conducted a set of experiments on load carrying capacity of scarf joint and scarf repair subjected to tension and compression loadings, respectively. A comparison of test results showed that the efficiency of scarf repair under compressive load was 20% higher than efficiency of the equivalent scarf joint under tensile load. Soutis and Hu [3] obtained the strength of a scarf repair and its equivalent scarf joint using the FEM and compared their simulation result with experiments of Jones and Graves [2]. Harman and Wang [4] developed an analytical technique to optimize design of isotropic adherends of scarf joints and validated their method using the FEM. Gunnion and Herszberg [5] adopted a thin slice model of a scarf joint with solid elements to study influence of laminate thickness, stacking sequence, mismatched adherends, adhesive thickness, and overply laminates on adhesive stresses. Wang and Gunnion [6] experimentally obtained the tensile strength of scarf joints of laminates $[0/45/-45/90]_{2s}$ and $[90/-45/45/0]_{2s}$, followed by a simulation based on the Generalized Plane Strain assumption and an elastic-perfectly plastic behavior for adhesive. Utilizing Abaqus software, plane strain solid elements, and a cohesive mixed-mode damage model for adhesive bonds, Campilho et al. [7] simulated two-dimensional tensile-loaded scarf CFRP joints of unidirectional laminate with various scarf angles. The obtained shear and peel stress distributions were in excellent agreement with the analytical results presented by Erdogan and

Ratwani [8]. Campilho et al. [9] investigated buckling of scarf joint of cross ply laminates experimentally and numerically using plane stress solid elements of Abaqus software. Trapezoidal and triangular separation-traction laws were applied to the adhesive/adherends interface and laminate ply interfaces. Good correlations were reported between the numerical predictions and experimental results for the elastic stiffness, strength, and failure modes of the joints.

A 3D FEM of scarf repair was performed by Pinto et al. [10] using the Cohesive Zone Model for the adhesive/patch interface to study the influence of scarf angle and overplies on adhesive bond strength. Goh et al. [11] conducted a set of experiments to obtain the scarf joint tensile strength with different flaw sizes embedded in the bondline. Experiments were followed by simulation approaches, including average shear stress, Linear Elastic Fracture Mechanics, Virtual Crack Closure Technique, and CZM in Abaqus, to estimate the strength of the joints numerically. Their results showed the CZM can accurately predict the strength of flawed and perfectly bonded scarf joints. Patel et al. [12] experimentally obtained the residual compressive strength of scarfed laminates with scarf angles of $6°$ and $10°$ for a variety of soft and stiff laminates. The results demonstrated that the reduction in the residual strength of a scarfed laminate, in comparison to its pristine laminate, depends on the laminate stiffness ratio. Yoo et al. [13] experimentally studied the static and fatigue strengths of scarf joints of unidirectional laminates. The influence of scarf angle, doubler overlap length, and patch size were investigated using tensile static tests. One million cycles fatigue test was also performed for two shallow scarf angles. The test results showed that the fatigue strength of the scarf joint specimen, in comparison to static strength, was significantly affected by the scarf angle. Cohesive failure was the dominant failure mode in specimens with steeper scarf angles, whereas mixed-mode failure was observed in specimens with shallower scarf angles.

Ridha et al. [14] performed a numerical study to analyze the progressive failure of scarf repair of 8 plies quasi-isotropic laminate. A stepped repair geometry was adopted to take advantage of assigning continuum shell elements to the model geometry. Continuum Damage Mechanics was applied to predict damage initiation and damage progression of the fiber and matrix, while one row of cohesive elements was used to model adhesive bond. The influence of the adhesive traction-separation criteria, adhesive strength, and softening law on the load-carrying capacity of scarf repair was investigated. Hayes et al. [15] experimentally obtained the tensile strength of scarf joint specimens with different disbond lengths located at the tip or the center of adhesive bondline under Room

Temperature, Hot-Wet, and Cold Dry conditions. The results showed that the strength of specimens under HW was not affected by the disbond length, whereas the residual strength of the scarf joint under RT and CD decreased at a faster rate than the bondline area reduction. Verified by the experiments presented by Hayes et al. [15], Hayes et al. [16] improved scarf joint strength prediction using Abaqus Explicit solver. The contribution of various failure mechanisms, including adhesive/adherend bond failure, adherend ply failure, plies delamination, and adhesive plasticity, to damage initiation and damage progression of scarf joints were investigated. A 3D thin slice of scarf joint with one element-size width under quasi-static tensile load was simulated. Hashin criteria were assigned to the composite materials to simulate fiber and matrix degradation. An elastic-perfectly plastic behavior was assigned to the adhesive to model its degradation and failure. For laminate $[45/0/0/-45/90]_{3s}$, the damage sequence analysis validated by experiments, showed that the damage initiated at the $45°/90°$ interface and progressed towards the adhesive/adherend bondline and eventually caused separation of the bondline.

Pitanga et al. [17] experimentally investigated a ply-wise variable scarf angle to reduce the removal of damaged laminates. The $0°$ plies were scarfed with 1:20 scarf ratio and the $45°$ and $90°$ plies were scarfed with 1:2 scarf ratios. The results showed this scarfing method can achieve 64% of tensile strength of the straight scarf with 1:30 scarf ratio while reducing the scarf removal by 60%. Roy et. al. [18] obtained the tensile strength of scarf joints experimentally and numerically. Scarf joints were tested at $25°C$, and $75°C$. The tensile strength of specimen at $75°C$ showed 86% lower strength than that ones at $25°C$. Finite Element Analysis using cohesive elements were conducted for 4 different 24 plies quasi- isotropic laminates, showed the joints strength varied up to 15%. Vadean et al. [19] investigated the optimized shape of scarf repair under uniaxial and biaxial tensile loads at different loading ratios using FEM. Their results showed the elliptical scarf patch allows removing up to 41% less of the parent structure in comparison to circular patch. The optimum scarf geometry is dependent on the loading ratio, when $0 \le \frac{\sigma_y}{\sigma_x} \le 0.25$, the $\frac{b}{a} = 0.25$ and when the $0.25 \le \frac{\sigma_y}{\sigma_x} \le 1$, the $\frac{b}{a} = \frac{\sigma_y}{\sigma_x}$. Sonat and Ozerinc [20] investigated the failure behavior of woven CFRP scarf joints with scarf angles of $1.9°, 2.8°$ and $5.7°$, experimentally and numerically. The Hashin criteria were used to model the intra-laminar failure of scarf joints. A good agreement between strength obtained from tests and simulation was reported. Their study showed that the dominant failure mode for scarf joint with $5.7°$ and $1.9°$ were respectively the cohesive failure and intra-laminar failure, while the

specimen with $2.8°$ scarf angle exhibited a mixed mode failure of the composite laminate and adhesive. Moreira et al. [21] conducted experimental and numerical works to study the static strength and high cycle fatigue life of a scarf joint of 16 plies UD CFRP, under three-point bending load. The experimental results that were obtained for scarf angle of $10°$ used to validate the finite element model which was a 2-D model consisting of CZM elements for adhesive. The results showed the fatigue life of a scarf repaired laminate was more affected by the scarf angle in comparison to the static strength. Hoang et al. [22] obtained the strength of scarf joint with the stacking sequence of $[45/-45/-45/0/90/0/45/-45/90/0]_S$, an over-ply layer, and four different scarf ratios ($1/5,\ 1/10,\ 1/20,\ 1/30$) using experiments and FEM. T-Sai Wu criteria and CZM were used to capture damage initiation and progression in composite laminate and adhesive. An exponential function used to fit the experimental data to correlate the scarf angles and failure loads. The results showed the discrepancies between experimental and simulation strengths depends on scarf angle. Tashi and Abedian [23] used Abaqus to simulate scarf repair and joint under uniaxial and equibiaxial loadings for various lay-ups and stacking sequences. The results showed ply shuffling in a quasi-isotropic laminate significantly affects the Stress Concentration Factor (SCF) of the adhesive bondline. The results raised a key design question: Should scarf joint/repair performance be a design criterion for composite laminates in early airframe design?

A general design guideline for most aerospace structures suggests considering the following recommendations when selecting a laminate stacking sequence [24].

- Stacking sequence have to be symmetric.
- Stacking sequence have to be balanced.
- No more than a limited number, generally four plies of the same orientation should be stacked.
- The difference between fiber orientations of consecutive plies should not exceed $45°$.
- No $0°$ ply on the free surface of the laminate is allowed.
- At least, 10% of plies should be placed in each direction of $0°$, $\pm 45°$ and $90°$.

The quasi-isotropic laminates with same number of plies are supposed to have similar strength under uniaxial load based on Classical Laminate Theory. But, as proven by experiments and numerical studies, their tensile strengths are different from each other due to the out-of-plane normal and shear stresses occurring at free edges of the laminates

[25-31]. Stress analysis of the free edge of the laminates showed that the positive out-of-plane normal stress at the edge causes the delamination and subsequently a lower strength, while negative out-of-plane normal stress at free edges suppresses the delamination [25, 27]. Ogihara et al. [29] experimentally determined the static and fatigue strengths of two quasi-isotropic laminates, $[0/45/90/-45]_s$ and $[45/0/-45/90]_s$, and showed that the latter has a lower strength. Tessema et al. [28] applied Damage Image Correlation to capture the damage initiation and propagation in three quasi-isotropic laminates: $[0/-45/45/90]_s$, $[0/-45/90/45]_s$, and $[0/90/45/-45]_s$. The laminate $[0/90/45/-45]_s$ exhibited the highest strength. Chen et al. [30] experimentally determined the tensile strength of six quasi-isotropic laminates presented in Table 1 and discussed the effect of free edge stresses on delamination using ANSYS. Hesabi et al. [31] obtained the strengths of six stacking sequences under a static tensile test and ranked the laminates based on their strengths, presented in Table 2. Wisnom et al. [32] experimentally obtained the strength of quasi-isotropic laminates with $[45/90/-45/0]_{ns}$ known as dispersed plies laminates and $[45_n/90_n/-45_n/0_n]_s$ known as blocked plies laminates with "n" includes 1, 2, 4, 8. As demonstrated by the experiments, laminates with dispersed plies exhibited much higher strengths than their blocked counterparts.

So far, many innovative scarf repair designs have been reported to increase the scarf repair strength and decrease the removal of pristine laminates. However, none of the previous research discussed on scarf repair performance as a parameter to design a composite laminate [33]. This study aims to analyze how the initial design of a pristine quasi-isotropic laminate is affected by scarf repair efficiency when the laminate is damaged and needs repair. FEM is used to obtain the ultimate tensile strengths of pristine laminates and their scarf joints. To lower computational costs, scarf joints are examined instead of repair geometry. Quasi-isotropic laminates and their scarf joints are studied to only measure the effect of stacking sequence on the strength of pristine laminate and its scarf joint.

2. Finite Element Model, Material Properties, Analysis Method

The 16 plies pristine laminates and their scarf joints with $5°$ scarf angle were modeled using ABAQUS. The material and geometric properties of the models are listed in Table 3, Table 4, and

Table 5. Pristine specimens under tensile loads were modeled as shown in Fig. 1. Composite plies were individually modeled using continuum shell elements and bonded together by cohesive contact interactions. 2D Hashin Failure criteria were used to model the composite failure modes. Cohesive damage properties based on the quadratic traction criterion for damage initiation and mixed-mode behavior for damage evolution were used to capture the plies delamination. Details of intralaminar and interlaminar failure properties are presented in

Table 6, Table 7, and Table 8. The ABAQUS Explicit solver was used to obtain strength of pristine laminates with time period of 0.01 second. The tensile load was applied by smooth step amplitude. A mass scaling factor of 10 was assigned to the elements to decrease the run time without compromising calculation accuracy. The performed mesh study which was in good agreement with mesh study results of Divse et al. [34] showed that the mesh size of $0.25mm \times 0.25mm$ is refined enough to have an accurate results.

A thin slice of the scarf joint specimen, which was extruded to the size of an element was considered as the scarf joint model. The front and rear surfaces of the specimen were constrained against the displacement normal to these surfaces to simulate conditions close to the plane strain assumption. The geometry and boundary conditions of the model are depicted in Fig. 2, and are similar to the simulation of Hayes et al. [16]. The simulation approaches considered for the scarf joint in the current study are verified by the simulation and experimental results of Hayes et al. [16]. The strengths of scarf joint specimens were obtained using two different modeling approaches. In modeling approach "A" only one cohesive interface was defined between one adherend and adhesive and strength of the joint specimens were obtained using Abaqus Standard. In modeling approach "B," using Explicit solver of Abaqus, cohesive contact properties were assigned to all the plies interfaces as well as the interfaces between plies and the adhesive to understand the influence of interlaminar failure on scarf joint performance. For simulation approach "B", the time period, mass scaling factor and amplitude of applied load were considered 0.01 second, 10 and smooth step as well. Neglecting other damage mechanisms that contribute to scarf joint failure is acceptable as Hayes et al. [16] reported that joint failure is substantially influenced by delamination propagated towards the adhesive/adherends interfaces. Based on previous study recommendation [16, 11, 35] the element size of a ply thickness with one row of elements through the thickness of each ply was considered to mesh composite plies. C3D8R and C3D6 elements were assigned to the plies. Four rows of solid elements were used to mesh the adhesive through its thickness. The damage stabilization coefficients required to stabilize the solutions were set to the 10^{-4} and 10^{-5} for composite material damage and cohesive damage, respectively.

2.1.Simulation Verification

The accuracy of the pristine laminate model was verified using the experimental results of Kechai et al. [36]. The strength of the pristine laminate with the $[0]_4$ lay-up was considered for the verification. The cohesive contact and composite failure properties were borrowed from the work of Divse et al. [34] who verified the experiments of

Kechai et al. [36]. The strengths predicted by current study and the experimental results of Kechai et al. [36] shows good agreement as depicted in Fig. 3. To investigate the scarf joint model accuracy, the experiment and simulation results of Hayes et al. [16] for a scarf joint with a $3°$ scarf angle were considered. Comparison of the strength results obtained by Hayes et al. [16] and the strengths obtained by the simulation approaches "A" and "B" are presented in Fig. 4. There is a very good agreement between the current simulation results and those of Hayes et al. [16] when 1 cohesive interface between adhesive/adherends was defined. However, assuming only one cohesive interface to simulate scarf joint failure leads to strength overestimation. The results obtained from approach "B" is in a very good agreement with experimental result of Hayes et al. [16]. However, a slight difference between simulation approach "B" and Hayes et al. [16] is observed which can be caused by the discrepancy between load amplitude, mass scaling factor, and density assumed in these two models. Moreover, Hayes et al. [16] considered all damage mechanisms contributing to scarf joint failure, while the current simulation was limited to interlaminar and adhesive/adherend interface failure modes.

2.2.Strength of Pristine Laminates

The Last Ply Failure criterion was considered to determine the ultimate tensile strength of the pristine laminates. Despite the fact that LPF is equivalent to the unstable growth of damage and large deformations of the composite laminate, it was intended to have a common understanding of failure of the pristine laminates.

The considered stacking sequences did not necessarily follow the composite laminate design guidelines. The stress-strain curve of 16 plies laminates is presented in Fig. 5. The quasi-isotropic laminates, before damage initiation, behaved similarly in the region of elastic loading, while their differences commenced as the interlaminar damages were initiated and propagated through the laminates. Reported in previous studies [25-31], the free edge stresses that vary with ply placement are responsible for the strength discrepancies of quasi-isotropic laminates under tensile loads. Ranking of quasi-isotropic laminates according to their ultimate tensile strengths are presented in Table 9. Considering Fig. 5, the difference in strength for laminate $[45/0/0/-45/90/-45/90/45]_s$ is highly distinguishable compared to the others. This could be explained by the two neighboring $0°$ stiff plies close to the free surface. Interestingly, the results for laminate $[0/45/-45/90]_{2s}$ shows that the effect of neighboring stiff plies is much higher than having the $0°$ plies on the free surface. As Fig. 5 shows, $[0/45/-45/90]_{2s}$ behaves almost the

same as the 16 plies laminate with $0°$ ply closest to the plane of symmetry (i.e. $[90/-45/45/0]_{2s}$). The reason could be in load carrying compensation that the $0°$ ply inside the laminate provides for the failed $0°$ ply on the free surface.

The simulation results presented in Table 9 are in good agreement with the trend reported by Wisnom et al. [32], who demonstrated that a quasi-isotropic laminate with dispersed plies has a higher tensile strength than a quasi-isotropic laminate with blocked plies.

2.3.Strength of Scarf Joint Model

2.3.1. Strength Prediction with 1 cohesive interaction (Approach "A")

Following the approach "A," tensile strength of scarf joints of 16 plies laminates were obtained when only one of the interfaces between adherends and adhesive considered as cohesive interface. The scarf joint failure was dependent solely on the failure of adherend/adhesive interface. The tensile strengths and contour plots of cohesive damage propagation through the interface of the adhesive/adherend are presented in Fig. 6 and Fig. 7. As shown and Fig. 6, the stacking sequence significantly affects the tensile strength of the scarf joints of quasi-isotropic laminates.

2.3.2. Strength Prediction with all cohesive interaction (Approach "B")

To gain insight into the interlaminar damage influence on scarf joint performance, tensile strengths of scarf joints were also obtained using approach "B." The results are shown in Fig. 8. The presented results in Fig. 8 confirm that the recommended design guidelines for stacking sequence do not necessarily are in favor of strength recovery of scarf joints. The scarf joints with $0°$ ply next to the symmetry plane do not show a good strength. Worth to mention that the scarf joint $[45/0/0/-45/90/-45/90/45]_s$ showed the worst strength among all the laminates. This is explained by neighboring effects of two $0°$ stiff plies close to the free surface.

The guideline recommendation of keeping the angle difference between neighboring plies to $45°$ is not effective for enhancing the strength of scarf joints. As shown in Fig. 8, the scarf joints with stacking sequences of $[45/0/90/-45]_{2s}$ and $[45/-45/0/90]_{2s}$ have higher strengths than stacking sequence of $[45/0/-45/90]_s$, despite not meeting the minimum angle difference rule. Moreover, the scarf joint $[45/-45/0/90/90/0/-45/45]_s$, despite having a stacking sequence with $0°/90°$ neighboring plies, ranked 3rd among the scarf joints.

According to Table 10, strengths of $[0/45/-45/90]_{2s}$, $[-45/90/90/45/0/45/0/-45]_s$ and $[45/0/0/-45/90/-45/90/45]_s$ obtained from approaches "A" and "B" are close, revealing that dominant failure mechanism of these stacking sequences is adhesive/adherend failure.

Because several quasi-isotropic stacking sequences were studied here and a one-by-one investigation of their damage initiation and progression is beyond the scope of the current study, the failure mechanism investigation is limited to stacking sequences with the lowest and highest tensile strengths.

The cohesive damage initiation and propagation for scarf joint of $[-45/45/0/90]_{2s}$ are presented in Fig. 9. Cohesive damage began at the tip of the $0°$ ply and was then slowly propagated. Following the increase in the applied load, disbond occurred at the adherends/adhesive interfaces adjacent to the $0°$ ply tips. Delamination observed between the $0°$ and $45°$ plies of the left adherend and the $0°$ and $90°$ plies of the right adherend. Increasing the applied load caused adherend/adhesive disbond resulted in final failure. As shown in Fig. 10, the failure of the scarf joints of the $[45/0/0/-45/90/-45/90/45]_s$ stacking sequence was expectedly driven by the high SCF produced at the tip of the $0°$ plies. The disbond that occurred at the tip of the $0°$ plies rapidly propagated along the bondline and caused the final failure.

A comparison of the damage initiation and propagation of the upper and lower ranks of the understudied stacking sequences in scarf joints confirmed that the plies placement, even in quasi-isotropic laminates, significantly affects joint performance. Ply placement in a quasi-isotropic laminate can cause premature failure of the adhesive/adherends bondline, whereas the composite adherends are still capable of bearing extra load. On the other hand, there are stacking sequences of quasi-isotropic laminates that can provide a more uniform stress field in the joint which leads to global failure of the joint, where the capacity of composite adherends also contributes to carrying the applied load. Although the analysis of damage initiation and damage progression in scarf joints is a broad and interesting topic that requires further study, it is not the primary objective of the current research. Instead, the focus of this failure analysis is to address the limitations of the current design procedure for composite laminates and its impact on their repair process, while also providing new insights into the design and optimization of composite laminates.

3. Discussion

Referring to Table 10, the scarf joint performance of quasi-isotropic laminates is much more sensitive to ply placement than that of the pristine laminate. For the pristine laminates, the difference in ultimate tensile strength for the 1st and last ranked understudied stacking sequences is 22.5%, while this difference for the best and worst scarf joints is 125%.

Based on Table 10, the maximum strength ratio (scarf repair strength-Approach "B"/Pristine Laminate ultimate strength) is 52%. It is emphasized that the ratios are calculated according to the ultimate strengths obtained from the failure of the last ply of the pristine laminates, and they are limited to the discussed stacking sequences.

The large disparities in strength between the quasi-isotropic scarf joints and their corresponding pristine laminates indicate that the presence of an inclined thin layer of adhesive as a bonding medium, combined with plies placement, can remarkably influence the stress field adjacent to the bondline in a way that the strength recovery of the scarf repair is reduced beyond the expectations.

One of the most significant conclusions that can be drawn from Table 10 is that the influence of stacking sequence on the strength of pristine quasi-isotropic laminates is not the same for their corresponding scarf joints. In some cases, stacking sequence has a reverse effect on the strength of the pristine laminate and its scarf joint.

In a hypothetical scenario in which a quasi-isotropic laminate is required to carry tensile loads, the stacking sequence of $[-45/45/0/90]_{2s}$ is excluded from the potential candidate selection pool in the first stage of the laminate design. This is based on the recommended design guidelines, despite the fact that, the neglected stacking sequence showed the best tensile performance as a scarf joint rather than the other discussed stacking sequences (Table 10).

Early exclusion from the laminate selection pool can occur for $[45/-45/0/90/90/0/-45/45]_s$ with low tensile strength. The stacking sequence does not obey the design guidelines, because the placement of plies in a pristine laminate result in early delamination. As shown in Fig. 11 (a), the delamination of the pristine laminate of the stacking sequence occurred at 55% of the final failure load, resulting in premature failure of the laminate at a relatively low strength. Nevertheless, the scarf joint performance of the stacking sequence was comparatively high, ranked 3rd among the examined scarf joints. As shown in Fig. 11 (b), the disbond of the adhesive/adherends and

plies delamination initiated and propagated slowly. No disbonds or delamination was observed at 90% of the final failure load.

Among the examined stacking sequences, $[90/45/0/-45]_{2s}$ is the most favorable stacking sequence, as its tensile strength is ranked 1st among pristine laminates and 2nd in scarf joint specimens, implying that manufacturing a laminate with acceptable performance in its pristine and scarf joint configurations is not unlikely. To determine the global optimum for stacking sequences or provide new design guidelines for laminates, the design philosophy should include the acceptable repair performance of the composite structures, as the use of composite materials is growing in aerospace and other industries. Additionally, the Philosophy of Design for Repair (PDR) for composite laminates should also be considered for recycling, to minimize the impact on the environment after the service life of the parts.

The contradictory effects of the stacking sequence on the pristine laminate and its scarf joint warrant further investigation as it can affect the Repair, Maintenance and Overhaul program (MRO) of composite parts used in an airframe structure. Damage to composite structures during their design life is not unexpected as composites have a brittle nature and are susceptible to impacts. However, as proven by the current study, the performance of scarf repair can vary significantly with the stacking sequence. Thus, involvement of the repaired laminate performance in the design procedure of a composite laminate is necessary to avoid penalties when strength recovery by scarf repair is required for a damaged part.

The exclusion of stacking sequences that do not have an acceptable tensile performance at the early stage of a structural part design can result in difficulties with repair design and decision making on repairing or replacing the part. As demonstrated by the results in Table 10, most of the stacking sequences with reasonable tensile performance in their pristine shape that were probably kept in the selection pool showed a lower strength recovery as scarf joints. This means that the scarf joints of the selected laminates need shallower scarf angles to meet the DUL requirement. Traditionally, defined by aviation regulators and airworthiness authorities, the strength of adhesively bonded repair of a laminate is compared to the DUL, which is equivalent to the tensile strength of Open-Hole Tension specimens with the hole diameter of 6.35 mm of that particular laminate. The residual strength of the scarfed laminate is compared to Design Limit Load which is equal to $\frac{2}{3}$ of DUL. The shallower scarf angles impose greater removal of

pristine portions of the laminate, making it difficult to obtain approval for the scarf repair as the DLL requirement would not be met, which is obliged by airworthiness regulations for adhesively bonded repairs.

The controversial influence of scarf angle on the DUL and DLL is a complicated condition that can lead to the following decisions: a) approval of steeper scarf angles for scarf repair with probable use of a thick doubler to restore the laminate strength. However, thick doublers may raise additional concerns including a local increase in stiffness and secondary bending effects. b) rejection of adhesively bonded scarf joints and probable use of bolted repairs for strength recovery of the damaged part, which may impose unwanted stress concentrations on brittle composite laminate. c) rejection of all potential repair candidates and replacement of the part, which may be environmentally and financially a costly decision.

Therefore, it is necessary to reconsider the design procedure of pristine composite laminates by considering their repair performance in the early stages of their design. A small defect, even a minor damage, or existence of an inclined thin adhesive film for joining purposes in composites, can disrupt the symmetry and balance of the laminate, creating unexpected couplings that may in turn change the laminate functional behavior. Such incidents can be detrimental in some cases by causing high SCF at ply stations in adhesively bonded repairs. Reported by Tashi and Abedian [23], the SCF for 3-Dimensional 8 plies scarf repair changes from 1.53 to 2.40 for various quasi-isotropic stacking sequences, while the SCF of an isotropic repair with $E = E_{11}$ of the composite lamina is 1.10. Their results demonstrated that a composite part under complex circumstances, such as adhesively bonded repair, is considerably different from an isotropic part. Considering the efficiency of repaired laminates as a design principle for stiffer laminates commonly used in the aerospace industry is much more emphasized by the authors of current study. This is because, as proven by Wang and Gunnion [6], scarf joints of stiffer laminates with higher bondline SCF have less potential for strength recovery; therefore, a shallower scarf angle is required (meeting DUL). On the other hand, as demonstrated by Patel et al. [12], scarfed hole specimens of stiff laminates require steeper scarf angles to provide sufficient residual strength (meeting DLL). This makes it more conundrum to meet airworthiness regulations for the approval of scarf repair of stiff laminates.

To examine the concept of PDR, another FEM analysis was conducted. A new geometry as shown in Fig. 12 (a), was modelled with a width of one element under tension. The material, interface properties, plies, and adhesive thicknesses were the same as those in the scarf joint model. The failure analysis was limited to the disbonding of

adhesive/adherends by assigning cohesive behavior to the interfaces between the adhesive and adherends. The stacking sequence of $[-45/45/0/90]_{2s}$ was considered because it had the best scarf joint performance under tensile load among the discussed stacking sequences. This laminate has a higher chance of recovering the required strength when steeper scarf angle is required. The tensile strengths of the scarf repair cross-sections for scarf angles of $5°$ and $8°$ were obtained using Abaqus/Explicit, presented in Table 11 and Fig. 13.

As expected, the strength of the scarf repair cross-section for an $8°$ scarf angle is approximately 32% less than the strength of the $5°$ scarf repair cross-section. Assuming that the $8°$ scarf angle was steep enough to meet the DLL, adding doublers to the repair configuration was required to enhance the tensile strength of the $8°$ scarf repair cross-section to meet the DUL. Three different configurations of doublers, as presented in Table 11, were considered to enhance the load-carrying capacity of the scarf repair cross-section with an $8°$ scarf angle. The dimensions of the two-sided unsymmetrical doublers are schematically presented in Fig. 12(b). The ply thickness and material properties of the doublers were similar to those of the repair and parent structures. Thin layers of adhesive with 0.13 mm thickness were used to bond doublers to the top and bottom surfaces of the scarf repair cross-section. Cohesive contact was considered for all interfaces between adhesives and adherends. The tensile strengths of the repair-doubler configurations are shown in Fig. 13 and Table 11. The strength of the scarf repair cross-section with $8°$ scarf angle is 142 MPa lower than that of the scarf repair cross-section with a $5°$ scarf angle. However, the scarf repair cross-section with an $8°$ scarf angle of $[-45/45/0/90]_{2s}$ still yields a higher strength than some of the stacking sequences with a $5°$ scarf angle ranked in Table 10. Increasing the doubler thickness stiffened the repair. Moreover, two-sided doubler configurations, both symmetric and unsymmetric are more effective than a one-sided doubler in restoring the strength of a scarf repair cross-section. Nevertheless, none of the examined repair-doubler configurations for an $8°$ scarf angle, recovered the tensile strength up to a strength of $5°$ scarf angle of $[-45/45/0/90]_{2s}$ stacking sequence. The scarf repair-doubler configuration with an $8°$ scarf angle and stacking sequence of $[[-45/45/-45/45]-[-45/45/0/90]_{2s}-[45/-45]]$ restored the strength to 399.7 MPa, which is higher than the tensile strength of most of the understudied stacking sequences with a $5°$ scarf angle presented in Table 10. This example confirms that designing a pristine laminate considering its future repair performance can

enhance its chance of meeting DLL and DUL requirements when adhesively bonded repair of the laminate is needed.

It should be emphasized that no parametric study has been conducted on the design parameters of a doubler. Studying the DLL of scarfed composite laminates accompanied by probabilistic analysis is required to gain a better understanding of how the repairability of a composite laminate can affect its design procedure, as long as the major concern for adhesively bonded repair is the residual strength of the damaged part. In addition, a more comprehensive FEM analysis in association with experimental work that includes other loading conditions can lead to improved conclusions.

Afterwards, the authors did not emphasize any of the stacking sequences as the best possible one for repair performance, but insisted that the design procedure of composite laminates must include their repair efficiency as one of the design principles.

4. Conclusion

A slight change in balanced symmetric composite laminates produces a 3D complex stress field with a high SCF owing to the coupling of longitudinal and flexural stiffness matrices. Various stacking sequences of 16 plies quasi-isotropic laminates were studied to understand the effect of ply placement on the tensile strength of a pristine laminate and its scarf joint. Failure analysis of pristine laminates included the failure of composite materials utilized by Hashin criteria as well as delamination modeled by cohesive interactions between plies. The load carrying capacity of the equivalent scarf joints was obtained by two simulation approaches: A) cohesive interaction was only defined for one adhesive/adherend interface and B) cohesive interactions were defined for all the interfaces. The pristine composite laminates and their scarf joints were ranked based on their tensile strengths. The free edge effect caused up to 22.5% discrepancy between ultimate tensile strengths of various stacking sequences. The tensile strength of the scarf joints was highly affected by the ply placement when the discrepancy between the 1st ranked and the last ranked understudied stacking sequences was 122.5%. A stacking sequence with a higher tensile strength in the pristine configuration does not necessarily result in a higher performance of its scarf joint. In some cases, the stacking sequence that can be excluded from the selection pool in the first step of the laminate design, demonstrated higher tensile strength recovery in its scarf joint configuration. This observation led to the idea of considering the repair performance of a composite part in its design process (PDR) to decrease the risk of part replacement when

damage occurs. The selection of a stacking sequence whose scarf repair provides a higher strength recovery increases the probability of meeting the DUL and DLL requirements of airworthiness regulation for adhesively bonded repairs. To evaluate the accuracy of the idea, the tensile strength of a scarf repair cross section with an $8°$ scarf angle that was elaborated with one-sided and two-sided doublers were obtained. The results showed that the configuration with a steeper scarf angle carried equal or more tensile load than most of the understudied stacking sequences with a shallower scarf angle of $5°$. This example shows how seeing the scarf repair performance as a design consideration for a composite laminate can provide an opportunity for the approval of adhesively bonded repair. Scarfing damaged parts with steeper angles causes lower removal of the pristine portions of the laminate, thereby increasing the chance of meeting the DLL requirement. Concurrently restoring the strength and stiffness of the damaged part and satisfying the DUL requirement become feasible by utilizing a doubler-scarf configuration for the repair.

5. Funding

This research did not receive any specific grant from funding agencies in the public, commercial, or none-profit sectors.

6. Data Availability

Not Applicable

7. Authors Biography

Dr. Ali Abedian is an associate professor at aerospace engineering department of Sharif university of technology. His research interests and activities are focused on creep analysis of metal matrix composites, stress analysis of free surface damage of unidirectional composites, application of genetic algorithms (gas) to the optimum design of laminated composites, stress analysis of delamination phenomena in laminated composite, FEM analysis of super plasticity in composites, FEM analysis of contact problems, optimum material selection and Nano technology. In addition to Academia, he has actively worked in the industry in the field of design, manufacture and repair of composite structures, structural health monitoring and Life prediction and extension of metallic structures.

Samaneh Tashi is a PhD graduate of Sharif university of Technology. Her research activities and interests are focused on design and analysis of composite structures, mainly the adhesively bonded joints. In recent years, she has been working as an R&D project manager, an author of technical- financial proposals, and a lecturer of undergraduate courses.

8. References

[1]Katnam K.B., Da Silva L., Young T., "Bonded repair of composite aircraft structures: A review of scientific challenges and opportunities, Progress in Aerospace Sciences", 61, pp. 26-42, (2013).

[2]Jones J.S., Graves S., "Repair Techniques for Celion/LARC-160 Graphite/Polyimide Composite Structures", Rockwell international downey ca space transportation systems Div., (1984).

[3]Soutis C., Hu F., "Strength analysis of adhesively bonded repairs", In Recent Advances in Structural Joints and Repairs for Composite Materials, L. Tong, C. Soutis, pp. 141-72, Springer Nature BV, Dordrecht, Netherlands, (2003).

[4]Harman A.B., Wang C.H., "Improved design methods for scarf repairs to highly strained composite aircraft structure", Composite structures, 75, pp. 132-44, (2006).

[5]Gunnion A.J., Herszberg I., "Parametric study of scarf joints in composite structures", Composite structures, 75, pp. 364-76 (2006).

[6]Wang C.H., Gunnion A.J., "On the design methodology of scarf repairs to composite laminates", Composites Science and Technology, 68, pp. 35-46, (2008).

[7]Campilho R . D. S. G. de Moura M.F.S.F., Domingues J. J. M. S., "Stress and failure analyses of scarf repaired CFRP laminates using a cohesive damage model", Journal of Adhesion Science and Technology, 21, pp. 855-70, (2007).

[8]Erdogan F., Ratwani M., "Stress distribution in bonded joints", Journal of Composite Materials, 5, pp. 378-93, (1971).

[9]Campilho R.D., De Moura M., Ramantani D., et al., "Buckling behaviour of carbon–epoxy adhesively-bonded scarf repairs", Journal of Adhesion Science and Technology, 23, pp. 1493-513, (2009).

[10]Pinto A., Campilho R., De Moura M., et al., "Numerical evaluation of three-dimensional scarf repairs in carbon-epoxy structures", International Journal of Adhesion and Adhesives, 30, pp. 329-37, (2010).

[11]Goh J., Georgiadis S., Orifici A., et al., "Effects of bondline flaws on the damage tolerance of composite scarf joints", Composites Part A: Applied Science and Manufacturing, 55, pp. 110-9, (2013).

[12]Patel M., Daynes S., Wang C.H., "The Influence of Orthotropy and Taper Angle on the Compressive Strength of Composite Laminates with Scarfed Holes", Advanced Materials Research, Trans. Tech. Publ., pp. 178-84, (2014).

[13]Yoo J.-S., Truong V.-H., Park M.-Y., et al., "Parametric study on static and fatigue strength recovery of scarf-patch-repaired composite laminates", Composite structures, 140, pp. 417-32, (2016).

[14]Ridha M., Tan V., Tay T., "Traction–separation laws for progressive failure of bonded scarf repair of composite panel", Composite structures, 93, pp.1239-45., (2011).

[15]Hayes-Griss J., Gunnion A., Khatibi A.A., "Damage tolerance investigation of high-performance scarf joints with bondline flaws under various environmental, geometrical and support conditions", Composites Part A: Applied Science and Manufacturing, 84, pp. 246-55, (2016).

[16]Hayes-Griss J., Orifici A ,.Khatibi A.A., "An improved progressive failure modelling and damage tolerant design methodology for composite scarf joints with bondline flaws", Composites Part A: Applied Science and Manufacturing, 131, 105776, (2020).
[17]Pitanga M.Y., Cioffi M.O.H., Voorwald H.J., et al., "Reducing repair dimension with variable scarf angles", International Journal of Adhesion and Adhesives, 104, pp. 102752, (2021).
[18]Roy R., Kweon J., Nam Y., "Tensile strength of multi-angle composite laminate scarf joints with FEM", IOP Conference Series: Materials Science and Engineering, IOP Publishing, 784, 012007, (2020).
[19]Vadean A., Abusrea M., Shazly M., et al., "Improvement of scarf repair patch shape for composite aircraft structures", The Journal of Adhesion, 99, pp. 1044-70, (2023).
[20]Sonat E., Özerinç S., "Failure behavior of scarf-bonded woven fabric CFRP laminates", Composite Structures, 258, 113205 (2021).
[21]Moreira R., De Moura M., Silva F., et al., "High-cycle fatigue analysis of adhesively bonded composite scarf repairs", Composites Part B: Engineering, 190, 107900, (2020).
[22]Hoang V.-T., Lee D.-S., Nam Y.-W., et al., "Numerical Prediction of Failure Load of Scarf-Patch-Repaired CFRP Composite Using Damage Zone Model and Cohesive Zone Model', International Journal of Aeronautical and Space Sciences, 24, pp. 419-29, (2023).
[23]Tashi S., Abedian A., "A Comprehensive 2 Dimensional and 3 Dimensional FEM Study of Scarf Repair for a Variety of Common Composite Laminates Under In-Plane Uniaxial and Equibiaxial Loadings", International Journal of Adhesion and Adhesives, 103092, (2022).
[24]Irisarri F.-X., Laurin F., Leroy F.-H., et al., Computational strategy for multiobjective optimization of composite stiffened panels, Composite structures, 93 (3), pp. 1158-1167, (2011).
[25]Pagano N., Pipes R.B., "The influence of stacking sequence on laminate strength, Mechanics of Composite Materials", Springer, pp. 246-54, (1994).
[26]Smith P., Pascoe K., "The effect of stacking sequence on the bearing strengths of quasi-isotropic composite laminates", Composite Structures, 6, pp. 1-20, (1986).
[27]Stevanović M., Marković D., Pešikan-Sekulić D., "Effects of stacking sequence on the strength of cross-ply and quasi-isotropic carbon/epoxy laminates", Materials Science Forum, Trans. Tech Publ ,pp. 465-72, (2004).
[28]Tessema A., Ravindran S., Wohlford A., et al., "In-Situ observation of damage evolution in quasi-isotropic CFRP laminates", Fracture, Fatigue, Failure and Damage Evolution, Volume 7, Springer, pp. 67-72, (2018).
[29]Ogihara S., Takeda N., Kobayashi S., Kobayashi A., "Effects of stacking sequence on microscopic fatigue damage development in quasi-isotropic CFRP laminates with interlaminar-toughened layers", Composites Science and Technology, 59, pp. 1387-98, (1999).
[30]Chen J., Takezono S., Nagata M., et al., "Influence of stacking sequence on the damage growth in quasi-isotropic CFRP laminates", Journal of the Society of Materials Science, 50, pp. 178-85, (2001).
[31]Hesabi Z., Majidi B., Aghazadeh J., "Effects of stacking sequence on fracture mechanisms in quasi-isotropic carbon/epoxy laminates under tensile loading, Iranian Polymer Journal, 14(6), pp. 531-538 (2005).
[32]Wisnom M., Khan B., Hallett S., Size effects in unnotched tensile strength of unidirectional and quasi-isotropic carbon/epoxy composites, Composite Structures, 84, pp. 21-8, (2008).
[33]Orsatelli J.-B., Paroissien E., Lachaud F., et al., "Bonded flush repairs for aerospace composite structures: A review on modelling strategies and application to repairs optimization, reliability and durability", Composite Structures, 304, p. 116338, (2023).
[34]Divse V., Marla D., Joshi S.S., "Finite element analysis of tensile notched strength of composite laminates", Composite Structures, 255 p.112880, (2021).

[35]Wang C.H., Gunnion A.J., Orifici A.C., et al., "Residual strength of composite laminates containing scarfed and straight-sided holes", Composites Part A: Applied science and manufacturing, 42, 1951-61, (2011).

[36]Khechai A., Tati A., Guerira B., et al., "Strength degradation and stress analysis of composite plates with circular, square and rectangular notches using digital image correlation", Composite structures, 185, pp. 699-715, (2018).

Table 1. Tensile strength of T800H/Epoxy quasi-isotropic laminate by Chen et al. [30]

Table 2. Tensile strength of U.F.C200 carbon/epoxy quasi-isotropic laminates by Hesabi et al. [31]

Table 3. Summary of pristine laminate and scarf joint geometry

Table 4. Material Properties for unidirectional IM7/977-3[16]

Table 5. Room temperature material properties for FM 300-2 K Adhesive [16]

Table 6. In-plane material failure properties for a single ply of IM7/977-3 [16]

Table 7. Damage parameters of IM7/977-3 [16]

Table 8. Cohesive failure properties of IM7/977-3 [16]

Table 9. Tensile Strength of quasi- isotropic laminates

Table 10. Comparison of the simulation results for quasi-isotropic scarf joints and pristine laminates

Table 11. Scarf-Doubler configuration for quasi-isotropic scarf repair with $[-45/45/0/90]_{2s}$ stacking sequence

Fig. 1. Pristine laminates boundary and loading conditions

Fig. 2. Boundary and loading conditions of scarf joint model

Fig. 3. Comparison of current simulation strength perdition with experimental results of Kechai et al. [36] for $[0]_4$

Fig. 4. Comparison of current simulation results with results of Hayes et al. [16]

Fig. 5. Stress- Strain curve for pristine quasi-isotropic laminates

Fig. 6. Comparison of stress-strain curves of scarf joints of quasi-isotropic laminates obtained from Approach "A" model

Fig.7. Contour Plot of Cohesive Damage for adhesive/adherend interface of a quasi-isotropic scarf joint (Approach "A")

Fig. 8. Stress-Strain curve of scarf joints obtained from Approach "B" model

Fig. 9. Contour plot of cohesive damage parameter for $\left[-45/45/0/90\right]_{2s}$ at a) 80% of failure load, b) 90% of failure load, c) failure load d) Post failure (Approach "B")

Fig. 10. Contour plot of cohesive damage parameter for $\left[45/0/0/-45/90/-45/90/45\right]_s$ at a) 80% of failure load, b) 90% of failure load, c) failure load d)Post failure (Approach "B")

Fig. 11. a) Delamination initiation at 55% of final failure load for $\left[45/-45/0/90/90/0/-45/45\right]_s$ pristine laminate, b) Cohesive damage state at 90% of final failure load for $\left[45/-45/0/90/90/0/-45/45\right]_s$ scarf joint

Fig. 12. Schematic for cross section of a scarf repair a) without doubler, b) with two sided unsymmetric doublers

Fig. 13. Tensile strength of scarf repair cross section of $\left[-45/45/0/90\right]_{2s}$ stacking sequence for various Scarf-Doubler configurations

Table 1.

Stacking Sequence	Tensile Strength (MPa)
$[0/45/90/-45]_s$	804
$[0/45/-45/90]_s$	693
$[-45/0/45/90]_s$	675
$[-45/0/90/45]_s$	665
$[45/90/-45/0]_s$	657
$[45/90/0/-45]_s$	615

Table 2.

Stacking Sequence	Tensile Strength (MPa)
$[90/45/0/-45]_s$	486
$[45/0/-45/90]_s$	467
$[45/90/0/-45]_s$	476
$[90/0/-45/45]_s$	463
$[0/45/-45/90]_s$	432
$[-45/45/0/90]_s$	424

Table 3.

Pristine Laminate dimension	$100\ (mm) \times 25\ (mm)$
Scarf joint model (length $\times$ width)	$100\ (mm) \times 0.13\ (mm)$
Number of plies	16
Scarf angles	$5°$
Ply thickness	$0.13\ (mm)$
Adhesive thickness	$0.2\ (mm)$

Table 4.

Property	IM7/977-3
$E_1(GPa)$	168
$E_2 = E_3(GPa)$	9.86
$G_{12} = G_{13}(GPa)$	4.95
$G_{23}(GPa)$	2.944
$\upsilon_{12} = \upsilon_{13}$	0.33
υ_{23}	0.34
Density $\left(Tonne/mm^3\right)$	$1.57e^{-9}$

Table 5.

Property	FM 300 Adhesive
$E\left(\text{GPa}\right)$	1.577
υ	0.3
Density $\left(Tonne/mm^3\right)$	$8.75e^{-10}$

Table 6.

Failure Type	Symbol	(MPa)
Longitudinal Fiber Tensile Strength	X_t	2825
Longitudinal Fiber Compressive Strength	X_c	2275
Transverse Matrix Tensile Strength	Y_t	66
Transverse Matrix Compression Strength	Y_c	275
In-Plane Shear Strength	S_{12}	110
Out-of-Plane Shear Strength	S_{23}	130

Table 7.

$G_{ft}\left[kJ/m^2\right]$	$G_{fc}\left[kJ/m^2\right]$	$G_{mt}\left[kJ/m^2\right]$	$G_{mc}\left[kJ/m^2\right]$
100	100	0.22	0.22

Table 8.

Interlaminar Fracture Property	$G\left[kJ/m^2\right]$	$K\left[N/mm^3\right]$	$\sigma,\tau\left[N/mm^2\right]$

Mode I	0.22	10^5	30
Mode II	0.9	10^5	60
Mode III	0.9	10^5	60
Damage Initiation and Evolution Specifications			
Cohesive damage criterion	Quadratic traction		
Mixed Mode behavior	Power law $\eta = 1.5$		

Table 9.

Laminate Number	**Stacking Sequence**	**Tensile Strength (MPa)**
1	$[90/45/0/-45]_{2s}$	932.8
2	$[45/0/90/-45[_{2s}$	888.6
3	$[45/0/-45/90]_{2s}$	866.1
4	$[90/-45/45/0]_{2s}$	865.7
5	$[0/45/-45/90]_{2s}$	862.2
6	$[-45/45/0/90]_{2s}$	831.0
7	$[-45/90/90/45/0/45/0/-45]_{s}$	803.8
8	$[45/-45/0/90/90/0/-45/45]_{s}$	793.3
9	$[45/0/0/-45/90/-45/90/45]_{s}$	760.0

Table 10.

Stacking Sequence	**Nonlinear Static Solver**	**Abaqus Explicit Solver**	**Abaqus Explicit Solver**	**Repair strength/pristine laminate (Static) %**	**Repair strength/pristine laminate (Explicit) %**
	Scarf Joint	Scarf Joint	Pristine laminate		
	Approach "A"	Approach "B"			
	Tensile Strength (MPa)	Tensile Strength (MPa)	Tensile Strength (MPa)		
$[-45/45/0/90]_{2s}$	488.9	437.6	831.0	58.8	52.7
$[90/45/0/-45]_{2s}$	447.9	418.8	932.8	48	44.9
$[45/-45/0/90/90/0/-45/45]_{s}$	446.9	401.5	793.3	56.3	50.6
$[45/0/90/-45]_{2s}$	436.7	404.2	888.6	49.1	45.5
$[45/0/-45/90]_{2s}$	433.7	395.5	866.1	50.1	45.7
$[90/-45/45/0]_{2s}$	327.6	300.6	865.7	37.8	34.7
$[-45/90/90/45/0/45/0/-45]_{s}$	318.5	315.8	803.8	39.6	39.3

$[0/45/-45/90]_{2s}$	283.3	294.8	862.2	32.9	34.2
$[45/0/0/-45/90/-45/90/45]_{s}$	210.2	194.1	760.0	27.7	25.5

Table 11.

Scarf-Doubler Repair Configuration	Scarf Angle	Top Doubler	Bottom Doubler	Tensile Strength (MPa)
$[-45/45/0/90]_{2s}$ -5deg	5°	N/A	N/A	446.4
$[-45/45/0/90]_{2s}$ -8deg	8°	N/A	N/A	304.0
$[-45/45/0/90]_{2s}$ -8deg-1SD	8°	$[-45/45]$	N/A	339.7
$[-45/45/0/90]_{2s}$ -8deg-2SD-Symm	8°	$[-45/45]$	$[45/-45]$	381.2
$[-45/45/0/90]_{2s}$ -8deg-2SD-Unsymm	8°	$[-45/45/-45/45]$	$[45/-45]$	399.7

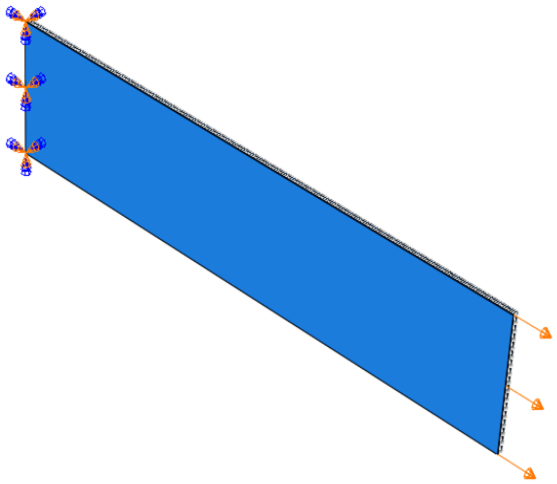

Fig. 1.

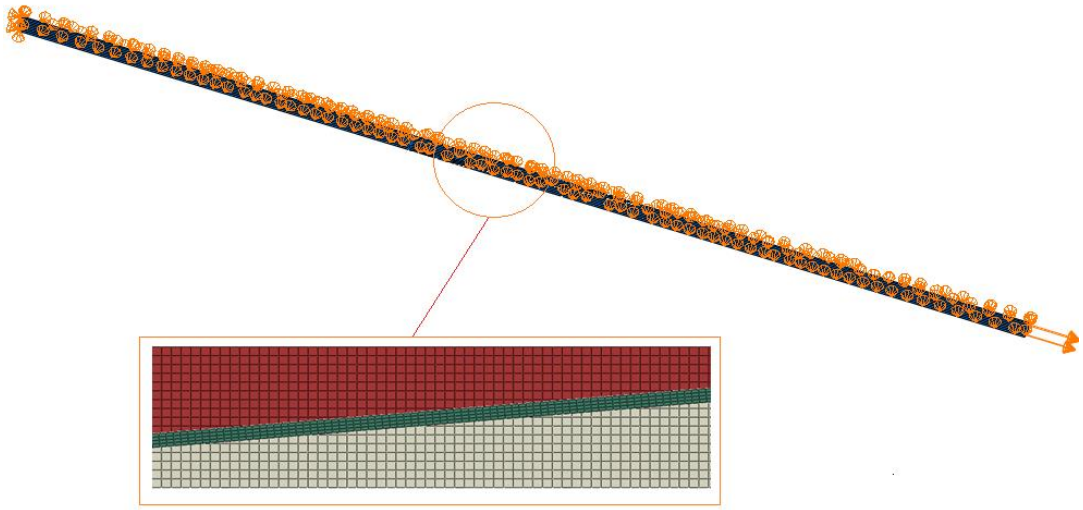

Fig. 2.

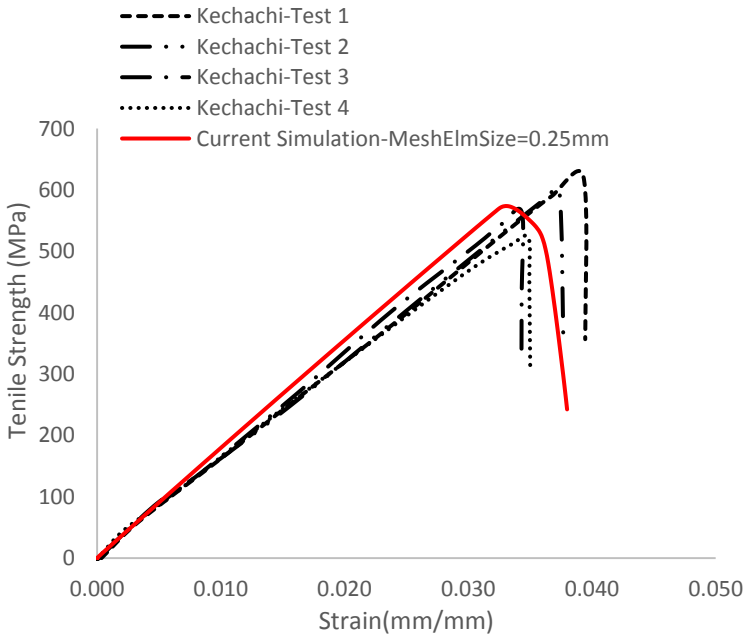
Kechachi-Test 1
Kechachi-Test 2
Kechachi-Test 3
Kechachi-Test 4
Current Simulation-MeshElmSize=0.25mm
Tenile Strength (MPa)
700
600
500
400
300
200
100
0
0.000
0.010
0.020
0.030
0.040
0.050
Strain(mm/mm)

Fig. 3.

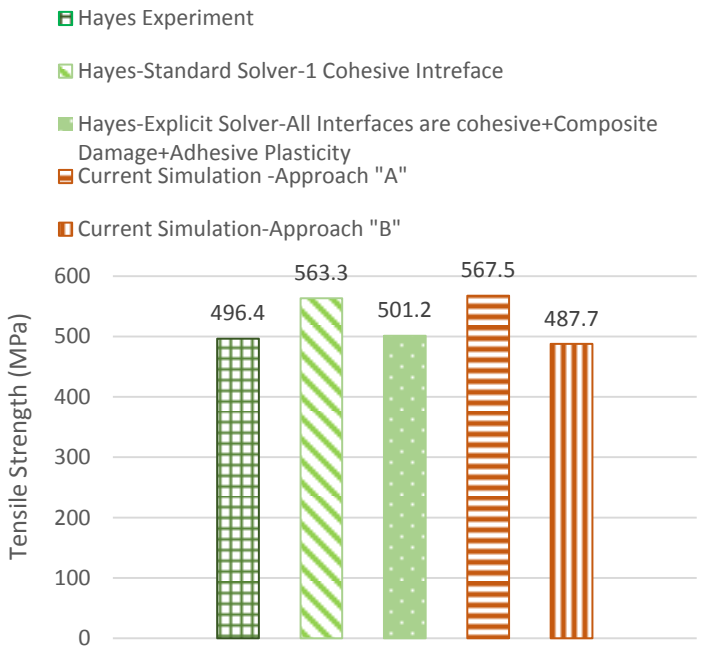
Hayes Experiment
Hayes-Standard Solver-1 Cohesive Intreface
Hayes-Explicit Solver-All Interfaces are cohesive+Composite Damage+Adhesive Plasticity
Current Simulation -Approach "A"
Current Simulation-Approach "B"
Tensile Strength (MPa)
600
500
400
300
200
100
0
496.4
563.3
501.2
567.5
487.7

Fig. 4.

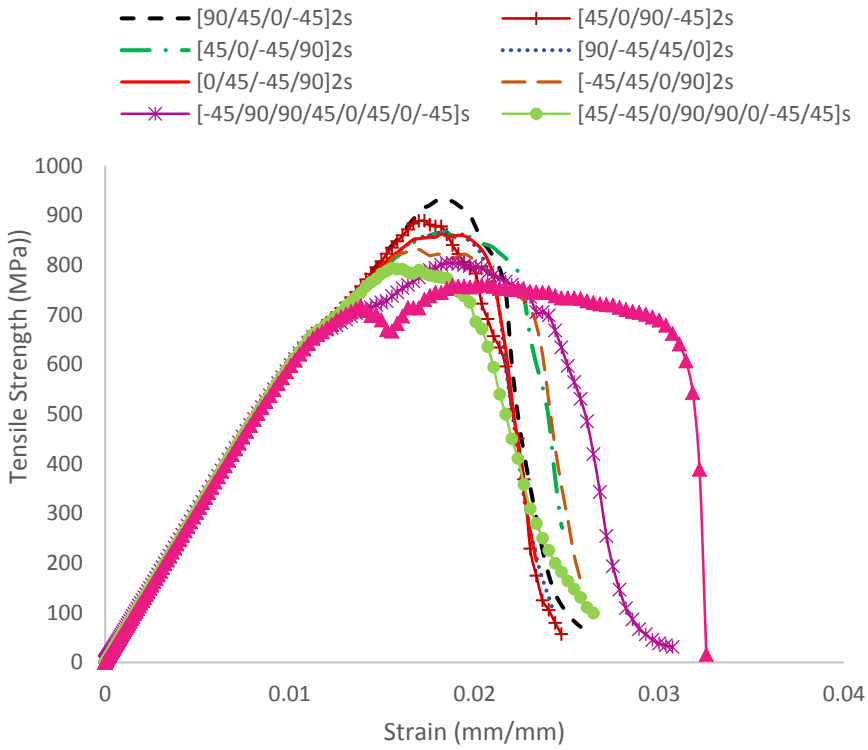
[90/45/0/-45]2s
[45/0/90/-45]2s
[45/0/-45/90]2s
[90/-45/45/0]2s
[0/45/-45/90]2s
[-45/45/0/90]2s
[-45/90/90/45/0/45/0/-45]s
[45/-45/0/90/90/0/-45/45]s
Tensile Strength (MPa))
1000
900
800
700
600
500
400
300
200
100
0
0
0.01
0.02
0.03
0.04
Strain (mm/mm)

Fig. 5.

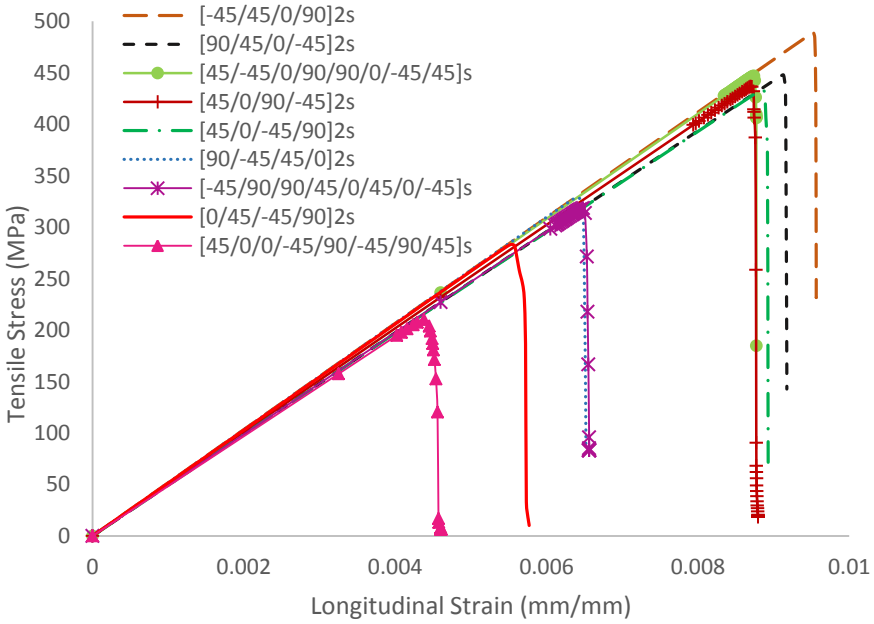
[-45/45/0/90]2s
[90/45/0/-45]2s
[45/-45/0/90/90/0/-45/45]s
[45/0/90/-45]2s
[45/0/-45/90]2s
[90/-45/45/0]2s
[-45/90/90/45/0/45/0/-45]s
[0/45/-45/90]2s
[45/0/0/-45/90/-45/90/45]s
Tensile Stress (MPa)
500
450
400
350
300
250
200
150
100
50
0
0
0.002
0.004
0.006
0.008
0.01
Longitudinal Strain (mm/mm)

Fig. 6.

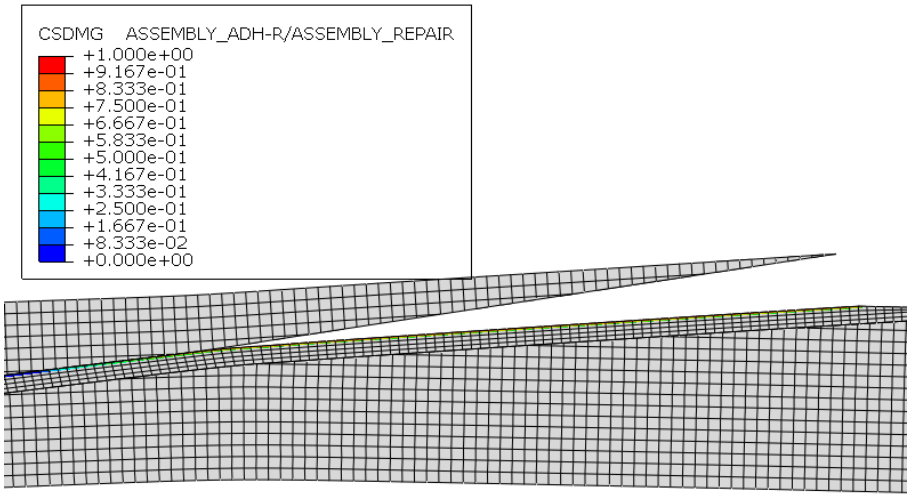
CSDMG ASSEMBLY_ADH-R/ASSEMBLY_REPAIR
+1.000e+00
+9.167e-01
+8.333e-01
+7.500e-01
+6.667e-01
+5.833e-01
+5.000e-01
+4.167e-01
+3.333e-01
+2.500e-01
+1.667e-01
+8.333e-02
+0.000e+00

Fig. 7.

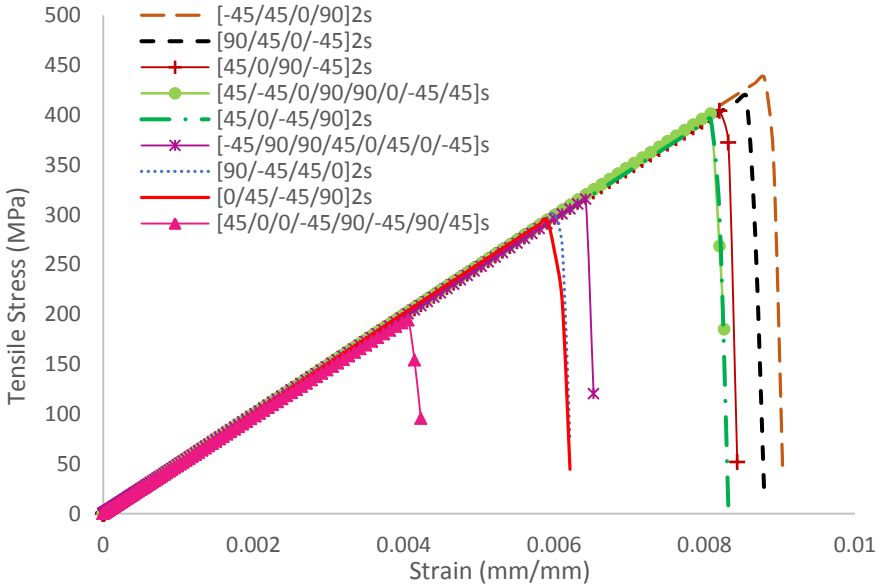
[-45/45/0/90]2s
[90/45/0/-45]2s
[45/0/90/-45]2s
[45/-45/0/90/90/0/-45/45]s
[45/0/-45/90]2s
[-45/90/90/45/0/45/0/-45]s
[90/-45/45/0]2s
[0/45/-45/90]2s
[45/0/0/-45/90/-45/90/45]s
Tensile Stress (MPa)
Strain (mm/mm)
500
450
400
350
300
250
200
150
100
50
0
0
0.002
0.004
0.006
0.008
0.01

Fig. 8.

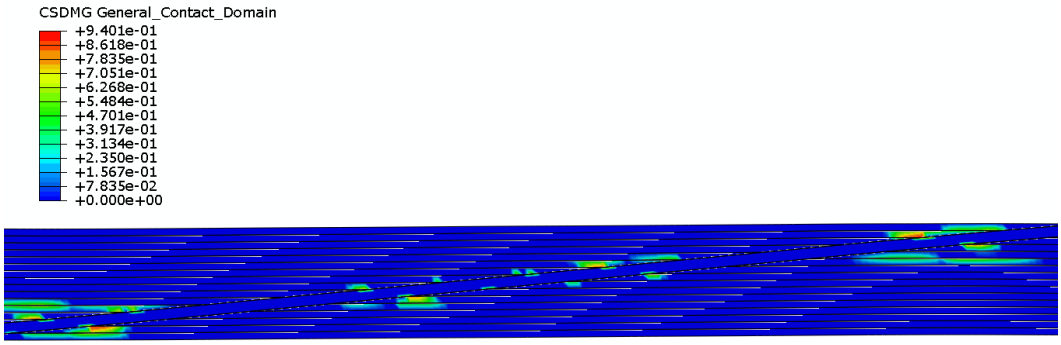
CSDMG General_Contact_Domain
+9.401e-01
+8.618e-01
+7.835e-01
+7.051e-01
+6.268e-01
+5.484e-01
+4.701e-01
+3.917e-01
+3.134e-01
+2.350e-01
+1.567e-01
+7.835e-02
+0.000e+00

(a)

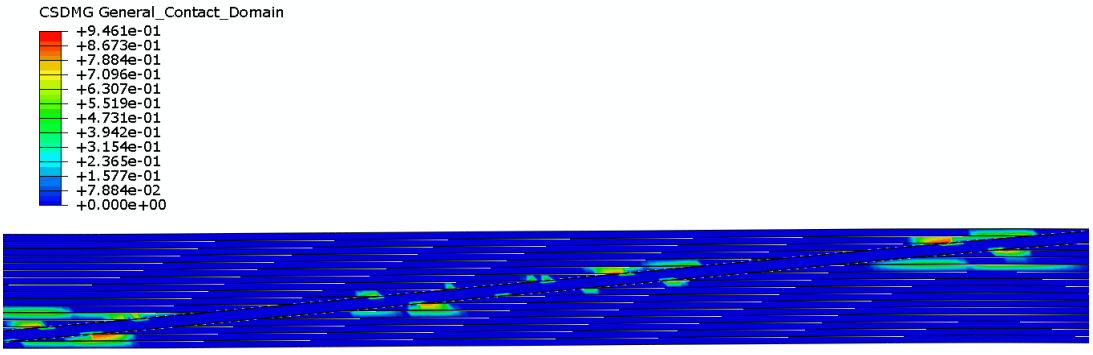
CSDMG General_Contact_Domain
+9.461e-01
+8.673e-01
+7.884e-01
+7.096e-01
+6.307e-01
+5.519e-01
+4.731e-01
+3.942e-01
+3.154e-01
+2.365e-01
+1.577e-01
+7.884e-02
+0.000e+00

(b)

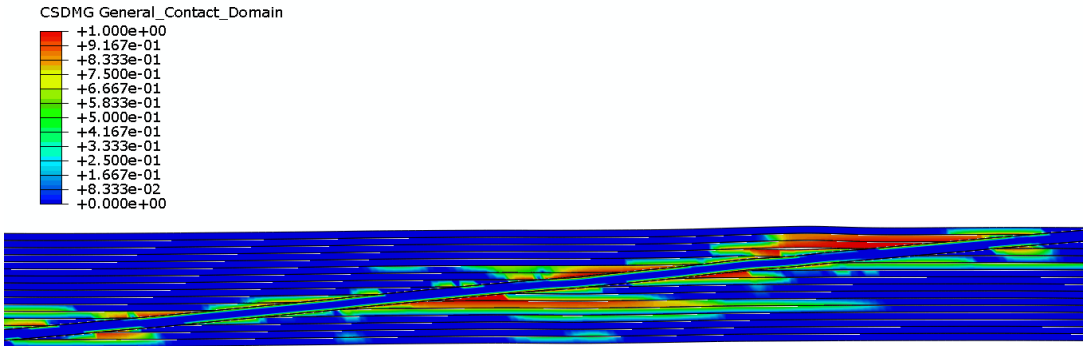
CSDMG General_Contact_Domain
+1.000e+00
+9.167e-01
+8.333e-01
+7.500e-01
+6.667e-01
+5.833e-01
+5.000e-01
+4.167e-01
+3.333e-01
+2.500e-01
+1.667e-01
+8.333e-02
+0.000e+00

(c)

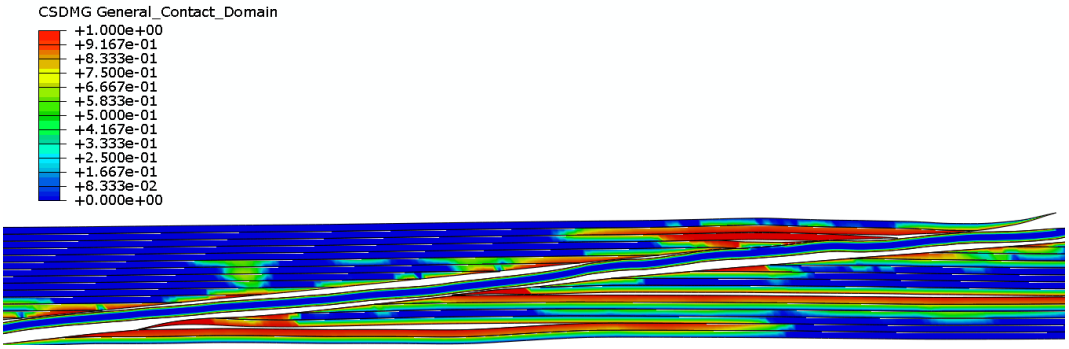
CSDMG General_Contact_Domain
+1.000e+00
+9.167e-01
+8.333e-01
+7.500e-01
+6.667e-01
+5.833e-01
+5.000e-01
+4.167e-01
+3.333e-01
+2.500e-01
+1.667e-01
+8.333e-02
+0.000e+00

(d)

Fig. 9.

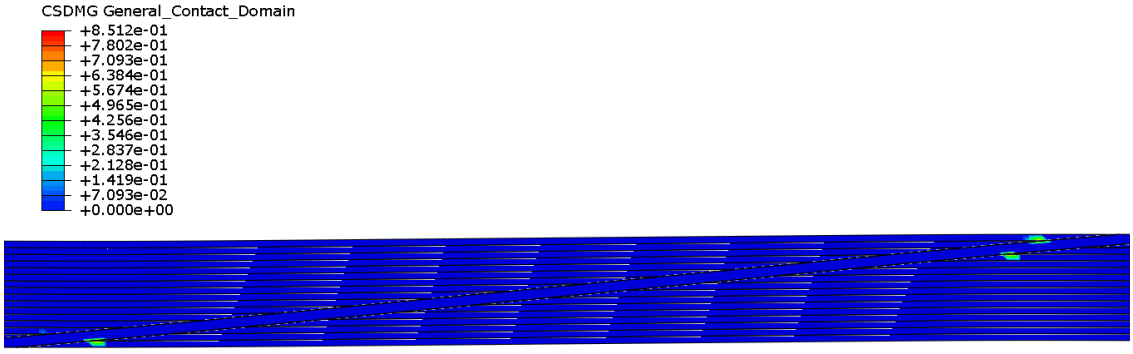
CSDMG General_Contact_Domain
+8.512e-01
+7.802e-01
+7.093e-01
+6.384e-01
+5.674e-01
+4.965e-01
+4.256e-01
+3.546e-01
+2.837e-01
+2.128e-01
+1.419e-01
+7.093e-02
+0.000e+00

(a)

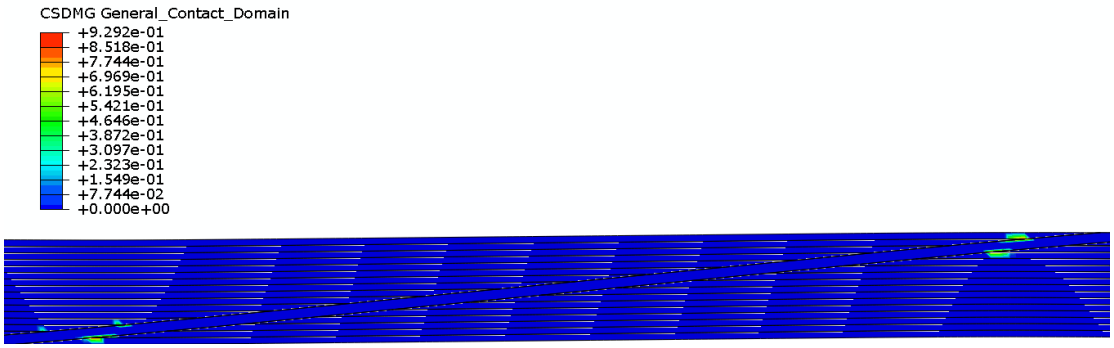
CSDMG General_Contact_Domain
+9.292e-01
+8.518e-01
+7.744e-01
+6.969e-01
+6.195e-01
+5.421e-01
+4.646e-01
+3.872e-01
+3.097e-01
+2.323e-01
+1.549e-01
+7.744e-02
+0.000e+00

(b)

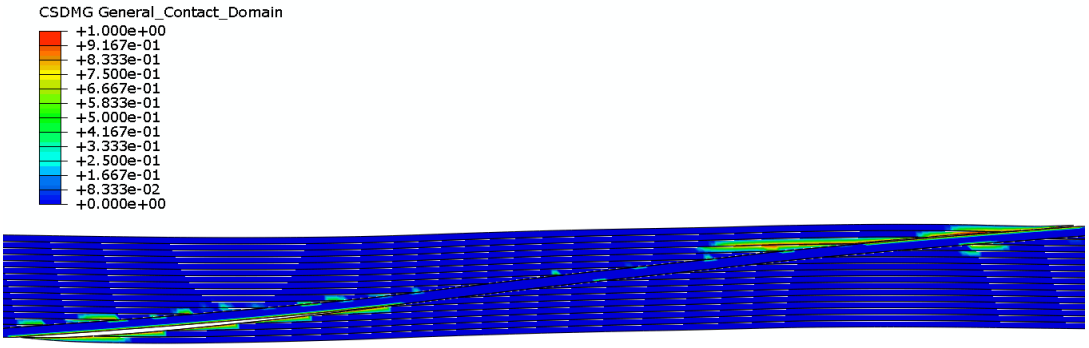
CSDMG General_Contact_Domain
+1.000e+00
+9.167e-01
+8.333e-01
+7.500e-01
+6.667e-01
+5.833e-01
+5.000e-01
+4.167e-01
+3.333e-01
+2.500e-01
+1.667e-01
+8.333e-02
+0.000e+00

(c)

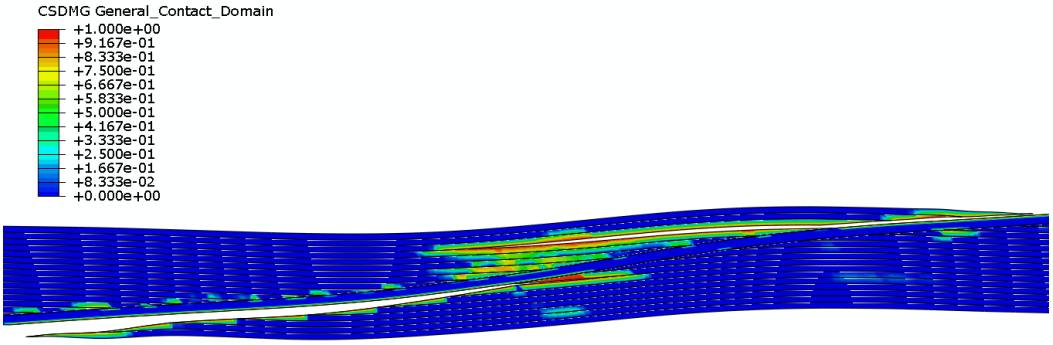
CSDMG General_Contact_Domain
+1.000e+00
+9.167e-01
+8.333e-01
+7.500e-01
+6.667e-01
+5.833e-01
+5.000e-01
+4.167e-01
+3.333e-01
+2.500e-01
+1.667e-01
+8.333e-02
+0.000e+00

(d)

Fig. 10.

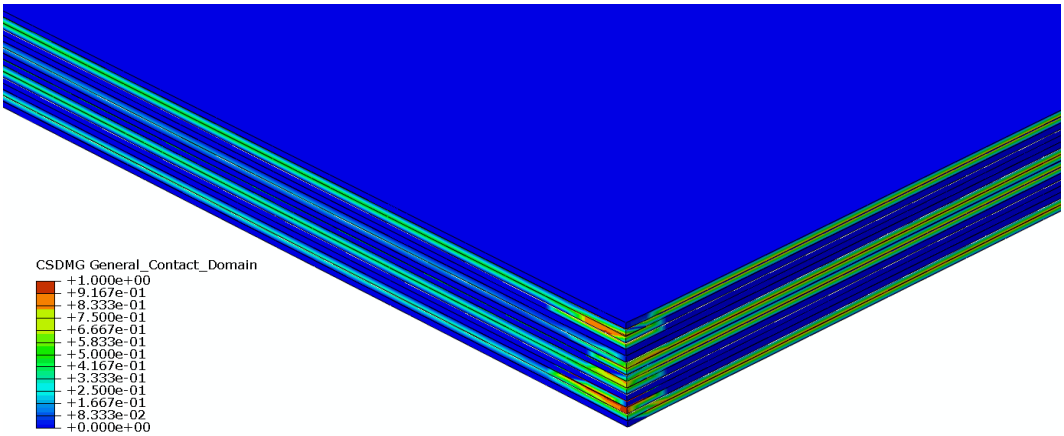

(a)

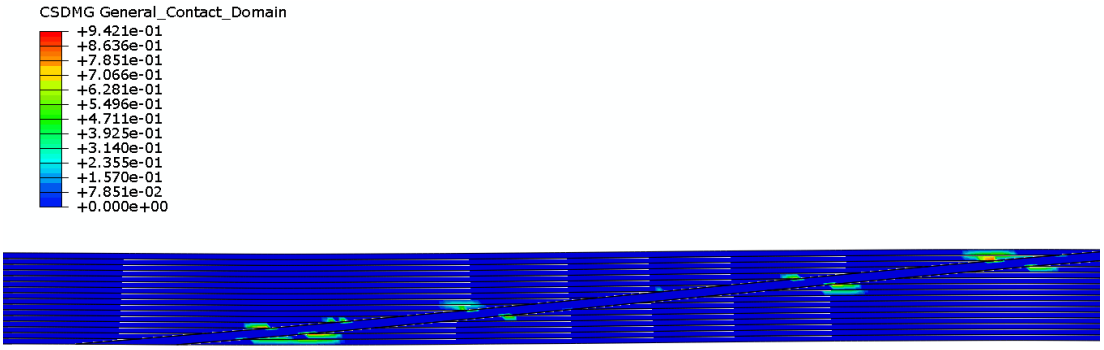

(b)

Fig. 11.

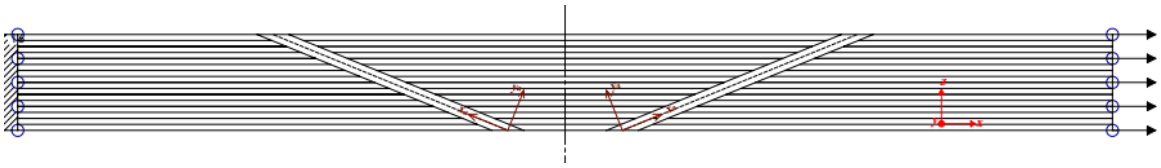

(a)

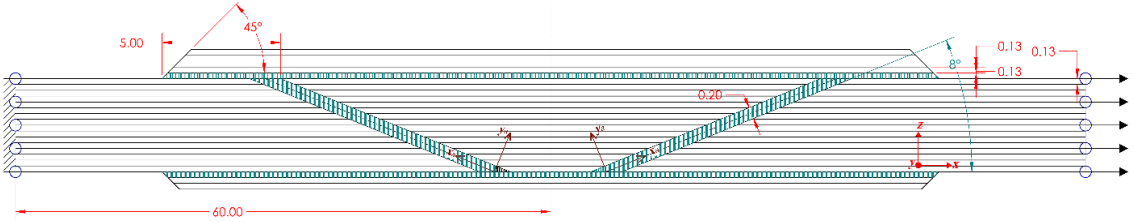

(b)

Fig. 12.

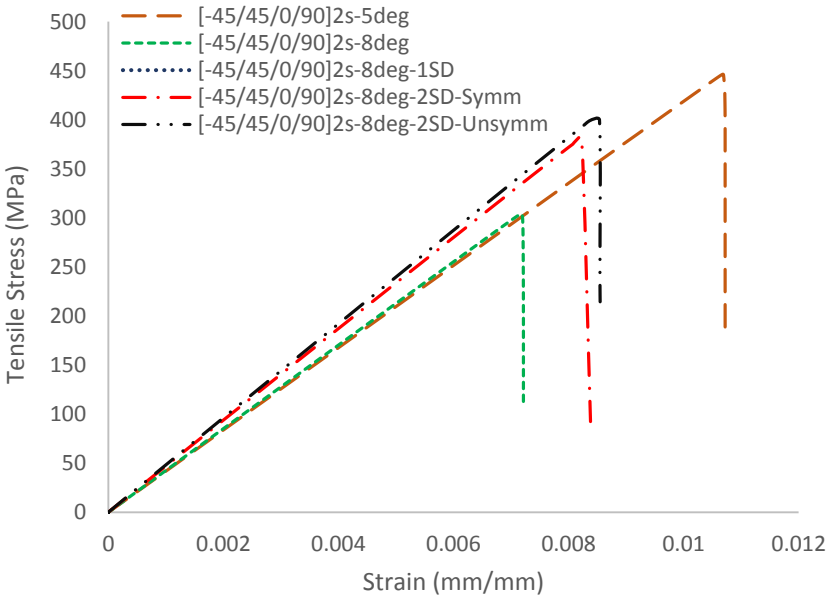
[-45/45/0/90]2s-5deg
[-45/45/0/90]2s-8deg
[-45/45/0/90]2s-8deg-1SD
[-45/45/0/90]2s-8deg-2SD-Symm
[-45/45/0/90]2s-8deg-2SD-Unsymm
Tensile Stress (MPa)
500
450
400
350
300
250
200
150
100
50
0
0
0.002
0.004
0.006
0.008
0.01
0.012
Strain (mm/mm)

Fig. 13.